Titania-Silica Catalysts for Lactide Production from Renewable Alkyl Lactates: Structure-Activity Relations

Journal:	*ACS Catalysis*
Manuscript ID	cs-2018-02216b
Manuscript Type:	Article
Date Submitted by the Author:	06-Jun-2018
Complete List of Authors:	De Clercq, Rik; Katholieke Universiteit Leuven, Centre for Surface Chemistry and Catalysis Dusselier, Michiel; Katholieke Universiteit Leuven, Poleunis, Claude; Université Catholique de Louvain, Institute of Condensed Matter and Nanosciences Debecker, Damien; Université catholique de Louvain, Institute of Condensed Matter and Nanoscience – IMCN, Division: MOlecules, Solids and reactiviTy – MOST Giebeler, Lars; Leibniz-Institute for Solid State and Materials Research, Institute for complex materials Oswald, Steffen; Leibniz-Institut fur Festkorper- und Werkstoffforschung Dresden eV, Makshina, Ekaterina; Katholieke Universiteit Leuven Sels, Bert; Katholieke Universiteit Leuven, M2S

Titania-Silica Catalysts for Lactide Production from Renewable Alkyl Lactates: Structure-Activity Relations

Rik De Clercq[1], Michiel Dusselier[1]*, Claude Poleunis[2], Damien P. Debecker[2], Lars Giebeler[3], Steffen Oswald[3], Ekaterina Makshina[1] and Bert F. Sels[1]*

[1]Centre for Surface Chemistry and Catalysis, KU Leuven, Celestijnenlaan 200F, 3001 Leuven, Belgium

[2]Institute of Condensed Matter and Nanosciences, Université catholique de Louvain, Louvain-la-Neuve, 1348 Belgium

[3]Leibniz-Institute for Solid State and Materials Research (IFW) Dresden e.V., Helmholtzstraße 20, D-01069 Dresden, Germany.

KEYWORDS: lactide, alkyl lactates, transesterification, Ti-Si catalysts, polylactic acid, Ti-zeolites

ABSTRACT: Different Ti-Si catalysts, *viz.* TiO_2 supported on amorphous SiO_2 or Si-MCM-41, TiO_2-SiO_2 xerogels and Ti-zeolites (TS-1 and Ti-beta) were compared in terms of activity and selectivity for the direct conversion of methyl lactate to lactide in the gas phase. Except for Ti-beta, all catalysts exhibit a high lactide selectivity of 88-92% at conversions below 50 %. From DR UV-VIS spectroscopy, it is evidenced that the catalytic activity of tetrahedral TiO_4 sites is higher than of polymerized TiO_5 or octahedral TiO_6 counterparts, irrespective of the catalyst structure, an analysis supported by ToF-SIMS measurements. A kinetic analysis shows that the catalytic activity is proportional to the number of vacant sites on the catalyst surface. Thus, the activity increase observed for tetrahedral TiO_4 sites may be attributed to an increased number of vacant sites (e.g. two for TiO_4, zero for TiO_6). Lactide productivity thus highly benefits from an increased dispersion of Ti-sites on the catalyst surface, and could be increased by a factor of 2.5 (up to 10 g_{LD} g_{cat} h^{-1}) when TiO_2 is dispersed on a Si-MCM-41 support, with higher surface areas than amorphous SiO_2 gels.

INTRODUCTION

To reduce the environmental impact that is related to the consumption of oil-based plastics, for instance the widespread contamination of the marine environment by microplastic debris[1,2], the continuous development of renewable and biodegradable alternatives remains a top priority.[3] Polylactic acid (PLA), a sugar-derived plastic, is currently a relatively well-established bio-based and recyclable synthetic polymer on the market and it is produced by the ring-opening polymerization (ROP) of lactide (LD), the cyclic dimer of lactic acid (LA).[4,5] To mitigate challenges related to the current industrial practice for LD production (e.g. two-step process, high energy costs, use of homogeneous catalysts)[6], an alternative process was proposed based on the shape-selective condensation of LA in an organic solvent.[7] Here, an aqueous LA feed is mixed with an organic solvent and H-beta zeolite under continuous water removal by evaporation. Despite high LD yields (85%), this process requires organic solvents and a continuous energy input to reflux the reaction medium. Therefore, we recently pioneered an alternative method for LD production based on the gas-phase transesterification of methyl lactate (MLA), providing a direct and continuous route to LD without the need of solvents (Scheme 1).[8] This ester-based process distinguishes itself from earlier reported gas-phase processes[9–12] for LD in the fact that no diluted aqueous LA feed is required. Indeed, the esters can be delivered to the reactor in pure form (no solvent), they are more volatile

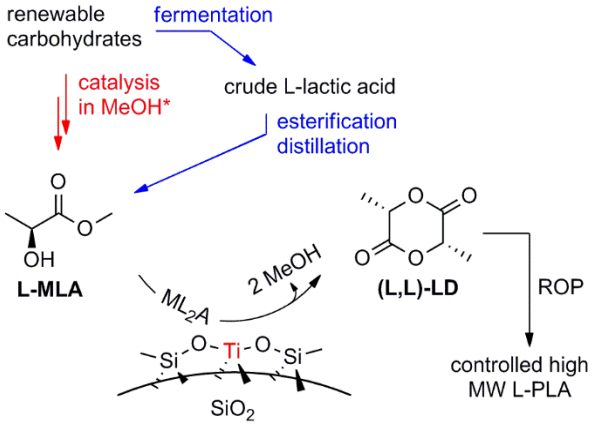

Scheme 1. Conversion of MLA to LD by a gas-phase transesterification over TiO_2/SiO_2 catalysts. *Note that while fermentation typically only produces the L-isomer of lactic acid, the catalytic production of MLA results in a racemic mixture, which requires subsequent separation of the L- and D-isomers (not shown for simplicity).[43]

than LA and less sensitive to autocatalytic or water-induced side-reactions.[13] An ester-based process also integrates well in the current PLA production scheme, since esters are intermediates in the LA purification step. Moreover, esters can be produced by emerging catalytic routes from carbohydrates in alcoholic media.[4,14,15] The beneficial use of alkyl lactates in gas-phase has also been demonstrated for producing methyl acrylate or acrylic acid through dehydration.[16–18] In our previous work[6], supported TiO_2/SiO_2 catalysts were, compared to other metal oxide catalysts, superior for gas-phase MLA transesterification and provide a LD selectivity up to 90%, with minor LD isomerization (≤ 7% meso-LD). A key feature of the catalyst was found in the presence of covalent Ti-O-Si bonds between the Ti active site and the SiO_2 support. Through DR UV-VIS spectroscopy analysis, the catalytic activity of the Ti-sites was correlated to the catalyst's corresponding band-gap energy (E_g). The value of this E_g is related to the number of nearest MO_x polyhedral neighbors and the number of bonds between each of those neighbors and can thus be used to monitor the evolution of the structure of supported species as a function of TiO_2 loading.[19] More specifically, we demonstrated that a lower average coordination of Ti seems indicative of a higher turnover frequency (TOF) of said active sites. The scope of this work is to investigate various Ti-Si catalyst structures, containing covalent Ti-O-Si bonds between the Ti sites and the silica-support, for the catalytic production of LD from MLA, and to correlate the specific activity of the Ti-sites to their corresponding average coordination geometry. The following catalyst structures are investigated: TiO_2 supported on amorphous SiO_2 or ordered mesoporous MCM-41, TiO_2-SiO_2 xerogels and two Ti-zeolites, *viz.* TS-1 and Ti-beta. Except for Ti-zeolites, different Ti-loadings were tested to change the corresponding average coordination of the Ti sites. A unique structure-activity relation is thus corroborated. Forthcoming insights are subsequently used to determine an optimal catalyst structure and to increase the productivity of lactide through the catalytic transesterification of alkyl lactates in the gas-phase.

EXPERIMENTAL SECTION

Material synthesis. Supported TiO_2/SiO_2 and TiO_2/MCM-41 catalysts were prepared by incipient wetness impregnation of a commercial, large-pore SiO_2 gel or self-made Si-MCM-41, respectively (synthesis: see Supporting Information). Prior to impregnation, the supports were dried overnight at 100 °C. An impregnation solution was prepared by adding Ti-isopropoxide to anhydrous isopropanol under an inert N_2 atmosphere, to avoid a rapid reaction of the Ti-isopropoxide with atmospheric moisture, which would form TiO_2. Then, the impregnation solution was immediately added dropwise to the support, this time under ambient air, while occasionally mixing the powder with a spatula. The chosen Ti-*i*Pr concentrations allow to reach the desired weight of TiO_2. The total volume of impregnation solution was equal to the pore volume of the support (as measured by N_2-physisorption). After impregnation, the powder was dried at 80 °C for 8 h, followed by calcination at 500 °C for 4 h (heating rate: 5 °C min^{-1}) in static air. TiO_2-SiO_2 xerogels (Aguado et al.[20]) were prepared by hydrolyzing tetraethylorthosilicate (TEOS), diluted in EtOH (molar ratio EtOH:TEOS = 2) with aqueous HCL (0.05M, molar ratio H_2O:TEOS = 1.2) at room temperature for 90 minutes. Then, the solution was cooled in an ice bath and the desired amount of Ti-*i*Pr, diluted in isopropanol under an inert N_2 atmosphere (mass ratio = 1:1), was added dropwise under continuous stirring. After 45 minutes, additional H_2O was added until a molar ratio of alkoxide (TEOS + Ti-*i*Pr):H_2O = 4 was achieved. The solution was stirred for 1 hour, after which the pH was raised slowly by the dropwise addition of aqueous NH_3 (1 M) until gelation occurred. The resulting gel was covered and let to rest for 24 h. Then, the gel was dried overnight at 80 °C, crushed into a fine powder and finally calcined at 500 °C for 4 h (5 °C min^{-1}). Ti-free SiO_2 xerogel was prepared according to the same procedure, but without the addition of Ti-*i*Pr. TS-1 (Carati et al.[21]) was prepared by adding 15.6 g of TEOS and 0.57 g of tetraethoxytitanate (TEOT) to 25.2 g of an aqueous tetrapropylammonium hydroxide (TPAOH) solution (14%). After hydrolysis and 3 h of aging at 40 °C, 31.5 g of H_2O were added. The resulting sol was transferred to a Teflon-lined stainless steel autoclave and heated at 180 °C under rotation for 15 h. Ti-beta (Blasco et al.[22]) was prepared by hydrolyzing TEOS in an aqueous solution of tetraethylammonium hydroxide (TEAOH, 35%) and H_2O_2. Then, TEOT was added and the solution was left under stirring to allow evaporation of ethanol and water. Afterwards, HF (40% in water) was added, along with additional water lost by evaporation. The resulting thick, yellow gel (with composition: TiO_2:60SiO_2:32.9NEt_4-OH:32.9HF:20H_2O_2:457.5H_2O) was transferred to a Teflon-lined stainless steel autoclave and was heated at 140 °C for 8 days under rotation (60 rpm). For both zeolites, the precipitate was filtered, washed thoroughly with H_2O, dried at 80 °C overnight and finally, calcined at 550 °C for 5 h (heating rate: 1 °C min^{-1}).

Catalyst characterization. N_2 physisorption measurements were performed on a Micromeritics Instruments Tristar 3000 at -196 °C. Prior to analysis, all samples were degassed overnight at 400 °C under a constant N_2 flow. Specific surface areas were calculated by the Brunauer-Emmett-Teller (BET) theory. Pore volumes were determined by the t-plot method on the desorption branch. Elemental analysis was performed by ICP-AES on an Ultima ICP-AES apparatus equipped with a Burgener atomizer and a radial optic detector (polychromator). Argon was the plasma source and carrier gas. Samples were prepared by acid digestion, *viz.* by dissolving 50 mg of powder in 0.5 mL of aqua regia and 3 mL HF (40%) for 3 h in a sealed PP bottle. Then, the acid was neutralized with 1.5 g of H_3BO_3 (dissolved in H_2O). The sample was then diluted to 100 mL in a volumetric flask, followed by further dilution if necessary. Powder XRD patterns were measured on a STOE Stadi P diffractometer using Cu $K\alpha_1$ radiation (monochromator: curved Ge(111) single crystal, λ = 0.15406 nm) and 180° position-sensitive image plate detector. FT-IR spectra were

measured under vacuum on a Bruker IFS 66v/s with a resolution of 4 cm^{-1} using a DTGS detector and an accumulation of 128 scans per spectrum. For this, the sample was ground, diluted with FT-IR grade KBr (1 wt% dilution) and pressed into a transparent film, which was placed in the sample holder. X-ray photoelectron spectroscopy (XPS) measurements were performed on a Physical Electronics PHI 5600 Cl equipped with a hemispherical analyzer, using Mg Kα radiation (1253.6 eV) at 400 W in an energy range of 0 – 1200 eV. Energy scale and binding energy were calibrated with Cu and Au foils at the binding energies of Cu 2p3/2 (932.67 eV), and Au 4f7/2 (84.00 eV), respectively. The sample chamber was held at a base pressure of around 10^{-10} mbar. High-resolution spectra were taken with a pass energy of 29 eV and a step size of 0.1 eV. All spectra were normalized in binding energy with respect to Si 2p = 103.3 eV. Elemental concentrations were calculated using the standard single element sensitivity factors provided by the PHI Multipak software package (version 9.5). Fits were performed with the PHI Multipak software applying a Shirley background algorithm. Raman spectra were measured at room temperature on a Horiba Jobin-Yvon HR800 Raman tool using a 532 nm laser with 50% ND filter. The exciting laser power was measured at the sample to be about 8 mW. The samples were pressed in self-supporting pellets. Multiple exposures (4x40 s) were taken for every spectrum and were software-corrected for spikes due to cosmic rays. Samples were measured under ambient conditions without any pretreatment. DR UV-VIS spectra were recorded on an Agilent Cary 5000 UV-VIS-NIR spectrophotometer at room temperature in the 4000-50000 cm^{-1} range. Pellets of the samples (250-500 μm) were loaded in a quartz U-tube/flow cell equipped with a UV-VIS transparent window. The samples were dried at 300°C under a N_2 flow for 1 hour (heating rate: 5°C min^{-1}) prior to measurement. The samples were kept under N_2 atmosphere during measurement. Background spectra were measured on dried $BaSO_4$ pellets (250-500 μm). The DR UV-VIS spectra were background corrected and the Kubelka-Munk function was used to display the data. The catalyst surface was analyzed by Time of Flight secondary ion mass spectrometry (ToF-SIMS)[23] with a TOF.SIMS[5] instrument from IONTOF GmbH. Sample powders were pressed onto adhesive part of Post-it® papers. A pulsed Bi_5^+ metal ion source was used to produce a primary beam at an acceleration voltage of 30 kV. An AC target current of 0.1 pA with a bunched pulse width lower than 1 ns was used. A raster of 128 x 128 data points over an area of 250 x 250 μm^2 was used. The total primary ion beam dose for each analysed area was kept below 7 10^{10} ions.cm^{-2}, ensuring static conditions. Lateral resolution of ~ 3 μm and mass resolution m/Δm >4000 at 29 *m/z* were maintained for spectra acquisition. Charge compensation was done by interlaced electron flood gun (E_k = 20 eV). Data analyses were carried out with the SurfaceLab software (version 6.5).

Catalytic reactions. Catalytic reactions were performed in a custom-built plug-flow fixed-bed reactor equipped with 6 parallel quartz reactors (length 480 mm, inner diameter of 4 mm) that can be operated individually. Reactors were loaded with 10-300 mg of catalyst (sieve fraction 250-500 μm), supported by quartz wool. If needed, quartz pellets (125-250 μm) were added to the catalyst bed to obtain a total bed weight of 300 mg. Prior to each reaction, catalysts were pretreated at 300 °C for 1 h (heating rate: 7 °C min^{-1}) under 20 ml min^{-1} of N_2, and was left to cool down to the desired reaction temperature. The feed solution consisted of 95 vol% L-MLA (97%, Acros Organics) and 5 vol% o-xylene (internal standard, Acros Organics), which was fed to an evaporation chamber (heated at 210°C) by a waters 515 HPLC pump at a rate of 0.005 ml min^{-1}. There, it was mixed with N_2 (20 ml min^{-1}) to obtain a gas mixture having a molar composition of 5.70/0.24/94.1 (L-MLA/o-xylene/N_2). The mixture was then passed through heated transfer lines (210 °C) to the reactor (220-280 °C) containing the catalyst bed. After the reaction, additional N_2 was added (30 ml min^{-1}) and the gas mixture was sent to the on-line GC for analysis.

Analysis. Effluent gases were analyzed by an on-line GC (HP 6890 series) equipped with an Agilent CP-SIL 24CB capillary column and FID detector (temperature program: 80 °C for 3 minutes, heating to 280 °C at a rate of 20 °C min^{-1} and remain isothermal for 1 minute). Product yields were calculated with o-xylene as internal standard, using response factors for each compound as determined via calibration curves with commercial standards. All data samples were taken after 2 hours on stream. Information on how conversion, selectivity, TOF, weight hour space velocity (WHSV) or space time yield (STY) are defined is given in the Supporting Information.

RESULTS AND DISCUSSION

Catalyst characterization. Three groups of Ti-Si catalysts with covalent Ti-O-Si bonds were synthesized between the Ti active site and the Si-support. The first group is TiO_2 supported on SiO_2, prepared through incipient wetness impregnation. Two types of SiO_2 support were used, *viz.* amorphous SiO_2 gel (S_{BET} = 287 m^2 g^{-1}) and ordered mesoporous MCM-41 (S_{BET} = 956 m^2 g^{-1}), denoted as TiO_2/SiO_2 and TiO_2/MCM-41 respectively. Here, all TiO_2 is deposited on the surface of the support (Figure 1A). The second type are TiO_2-SiO_2 xerogels (denoted as TiO_2-SiO_2), prepared through sol-gel syntheses where Ti is dispersed in the SiO_2 matrix instead of solely on the surface (Figure 1B). The third type are Ti-zeolites, *viz*. TS-1 and Ti-beta, with MFI and BEA topology, respectively, and wherein Ti is in tetrahedral coordination within the framework (Figure 1C). Except for the zeolites, various TiO_2 loadings were used. Their elemental composition, specific surface area/pore size and corresponding Ti-dispersion were measured through ICP-AES and N_2 physisorption (Table 1). TiO_2 loadings reported from here are the actual loadings as measured by ICP-AES. Powder XRD of TS-1 and Ti-beta showed the typical reflection patterns of MFI and BEA topology, respectively.[24] No reflections corresponding to anatase or rutile were observed, suggesting the absence of large crystalline TiO_2 particles, even at loadings of 30.4 wt% TiO_2 (Figure S1 in

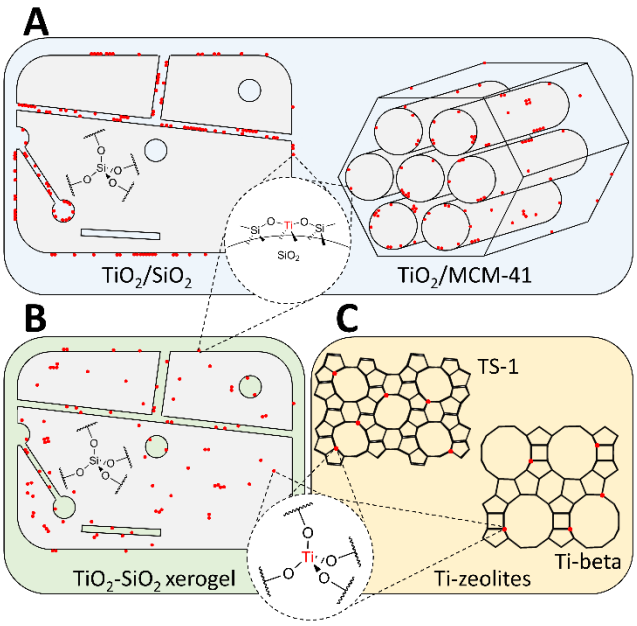

Figure 1. Schematic representation of different Ti-Si catalysts tested in this study. A) TiO2 supported on amorphous SiO2 gel (left) or Si-MCM-41 (right), B) TiO_2-SiO_2 xerogels and C) Ti-zeolites. Red dots schematically indicate the location of Ti-atoms. Note that only isolated Ti-species are shown for simplicity, though polymerized TiO_5 or TiO_6 species also could occur for supported catalysts and xerogels.

the Supporting Information). Raman spectroscopy is more sensitive toward identification of TiO_2 crystallites.[25] A small signal at ~148 cm^{-1} was observed only for the 20.1 wt% TiO_2/SiO_2, indicating the formation of small anatase crystallites at this loading (Figure S2). FT-IR spectra of the three groups of catalysts are presented in Figure 2. Amorphous SiO_2 and Si-MCM-41 exhibit a weak band at ~973 cm^{-1} from the symmetric stretching of Si-OH groups, as well as a band at ~810 cm^{-1} from the symmetrical Si-O-Si vibration.[26,27] The addition of titanium oxide species decreases the intensity of the 973 cm^{-1} band with the appearance of a new broad band at ~960 cm^{-1} indicative for Ti-O-Si bonds (Figure 2 A-C).[25,27–30] A sharper band is noticed at 960 cm^{-1} for the TS-1 zeolite (Figure 2D) while the same band is much weaker for Ti-beta, likely due to the lower Ti-loading compared to TS-1 (Table 1). Note that the intensity of the 960 cm^{-1} band is very weak for supported TiO_2/SiO_2, especially when compared to TiO_2-SiO_2 gels or TS-1, an observation reported by Gao et al.[27] TiO_2 surface dispersion in supported TiO_2/SiO_2 was investigated by XPS. Binding energy (BE) values of O 1s, Ti $2p_{3/2}$ and Si 2p are presented in Table 2.

Table 1. Sample composition, pore texture and Ti-dispersion of different Ti-Si catalysts.

	Catalyst[a]	wt% TiO_2[b]	Si/Ti	S_{BET} (m^2 g^{-1})	Ti atoms nm^{-2}	pore volume (cm^3 g^{-1})[c]
supported catalysts	SiO_2 support	0	-	287	0	0.931 (0.019)
	TiO_2/SiO_2 0.4 %	0.4	336	248	0.12	0.750 (0.019)
	TiO_2/SiO_2 1 %	1.1	120	220	0.38	0.687 (0.021)
	TiO2/SiO2 2 %	1.9	69	235	0.61	0.534 (0.020)
	TiO2/SiO2 5 %	4.7	27	268	1.32	0.702 (0.017)
	TiO2/SiO2 10 %	10.4	11	253	3.10	0.711 (0.018)
	TiO_2/SiO_2 20 %	20.1	5	255	5.94	0.533 (0.009)
	TiO_2/SiO_2 30 %	30.4	3	162	14.15	0.359 (0.008)
	(Si-)MCM-41	-	-	956	0	0.582 (0)
	TiO_2/MCM-41 0.05 %	0.05	2828	926	$3.8*10^{-3}$	0.585 (0)
	TiO_2/MCM-41 0.1 %	0.09	1444	922	$7.5*10^{-3}$	0.579 (0)
	TiO_2/MCM-41 1 %	0.9	157	944	0.07	0.593 (0)
	TiO_2/MCM-41 5 %	4.2	30	917	0.34	0.548 (0)
	TiO_2/MCM-41 10 %	8.4	15	766	0.83	0.372 (0)
	TiO_2/MCM-41 20 %	16.9	6.5	774	1.65	0.306 (0)
xerogels	TiO_2-SiO_2 1 %	0.8	165	748	-[d]	0.548 (0.022)
	TiO_2-SiO_2 5%	4.1	31	904	-[d]	0.632 (0.034)
	TiO_2-SiO_2 10%	7.05	18	643	-[d]	0.461 (0.010)
	TiO_2-SiO_2 20%	14.6	8	466	-[d]	0.257 (0.257)
Ti-zeolites	Ti-beta	0.4	348	411	0.07	0.206 (0.206)
	TS-1	2.85	45	324	0.66	0.158 (0.158)

[a]Percentages indicate theoretical wt% of TiO_2 that was intented before impregnation. [b]Actual TiO_2 wt% as determined by ICP-AES. [c]values between brackets correspond to the micropore volume only. [d]Ti is distributed within the gel instead of only on the surface, thus Ti atoms nm^{-2} can not be accurately calculated.

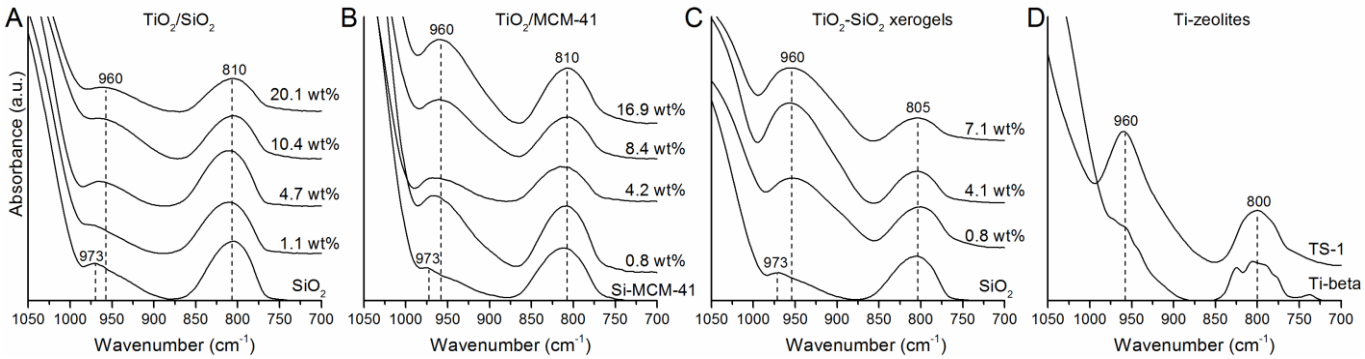

Figure 2. FT-IR spectra of A) TiO_2/SiO_2 B) TiO_2/MCM-41, C) TiO_2-SiO_2 xerogels and D) Ti-zeolites in the 700-1050 cm^{-1} region.

Table 2. Binding energies of Core Electrons for different titania-silica catalysts.

entry	catalyst	O 1s (eV)	Ti $2p_{3/2}$ (eV)	Si 2p (eV)
1	SiO_2	532.9		103.3
2	TiO_2/SiO_2 1.1 wt%	532.7 (97.4)[a] 529.5 (2.6)	459.4	103.3
3	TiO_2/SiO_2 4.7 wt%	532.5 (91.8) 529.5 (8.1)	459.2	103.3
4	TiO_2/SiO_2 10.4 wt%	532.6 (90.2) 530.2 (9.8)	459.1	103.3
5	TiO_2-SiO_2 4.1 wt%	532.5 (98.0) 529.4 (2.0)	459.6	103.3
6	TiO_2[b]	530.5	458.7	103.3

[a]Values in brackets indicate the area percentage of the band.[b]anatase

Compared to the O 1s signal of the SiO_2 reference (532.9 eV, entry 1), a second signal of O 1s may be resolved at ~529.5-530.2 eV (Figure S3) for TiO_2 containing samples, which increases with increased TiO_2 loading (entries 2-4). Simultaneously, a slight blue shift in BE values of Ti $2p_{3/2}$ are observed compared to anatase (entry 6). The blue shifts observed for the BE values of both O 1s and Ti $2p_{3/2}$ with respect to pure TiO_2 have been associated with the presence of Ti-O-Si bonds and confirm our FT-IR results.[25,27,31] A similar observation was made for TiO_2-SiO_2 mixed gels (entry 5). A comparison between surface and bulk atomic Ti/Si ratios (Figure 3) shows that, for TiO_2/SiO_2 catalysts, the catalyst surface is enriched with a disperse, amorphous TiO_2 phase up to loadings of 4.7 wt% TiO_2,without formation of anatase crystallites. At 10.4 wt% TiO_2 loading, the surface Ti/Si ratio is slightly lower than in the bulk, suggesting that 3D particle growth may already occur. At this loading, a surface Ti distribution of 3.1 Ti atoms nm^{-2} was calculated (Table 1), while the capacity for TiO_2 monolayers on SiO_2 are expected to be at 2.2-5.5 Ti atoms nm^{-2}.[27,32,33] For a TiO_2-SiO_2 xerogel containing 4.1 wt% at TiO_2, surface and similar bulk Ti/Si ratios, no surface enrichment of Ti occurs and points to homogenously distributed Ti already in the gel state. In order to obtain a deeper molecular insight in the surface chemistry of the catalysts, the latter have been analyzed by ToF-SIMS. Owing to its high surface sensitivity, ToF-SIMS has been shown to be extremely useful for the characterization of heterogeneous catalysts.[34,35] Here, a series of cations emitted from the catalyst outermost surface was followed to characterize the dispersion of Ti. Generally speaking, the amount of Ti detected at the surface is lower for the TiO_2-SiO_2 xerogels as compared to the impregnated catalysts (Figure S4). Indeed, in the case of sol-gel synthesis, part of the Ti species is expectedly located in the bulk of the gels and not at the surface. At high TiO_2 loadings, the total amount of Ti detected at the surface of the TiO_2/MCM-41 catalyst is lower than that detected on TiO_2/SiO_2. This observation suggests that TiO_2 accumulates at the external surface of the amorphous silica support with low surface area, while it gets more dispersed inside the available porosity of the MCM-41 support. Interestingly, the relative proportions of the different ions detected vary in the different sample series. A relatively high proportion of "Mono-Ti" ions (Ti^+, TiO^+, TiO_2H^+) and "Mixed Ti-Si" ions ($TiOSi^+$, TiO_2Si^+, TiO_3Si^+, TiO_4Si^+) is detected in the TiO_2-SiO_2 xerogels, accounting for the presence of highly dispersed Ti species incorporated into the silica matrix (Fig. S5 & S6). On the other hand, for TiO_2/SiO_2 and TiO_2/MCM-41 catalysts prepared by impregnation, "Poly-Ti" ions ($Ti_2O_2^+$, $Ti_2O_3^+$, $Ti_2O_4H^+$,

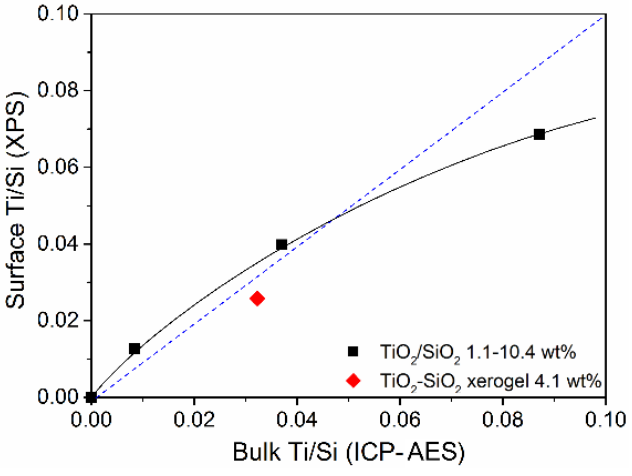

Figure 3. Surface Ti/Si composition (measured by XPS) versus bulk Ti/Si composition (measured by ICP-AES). The blue dotted line indicates where both are equal.

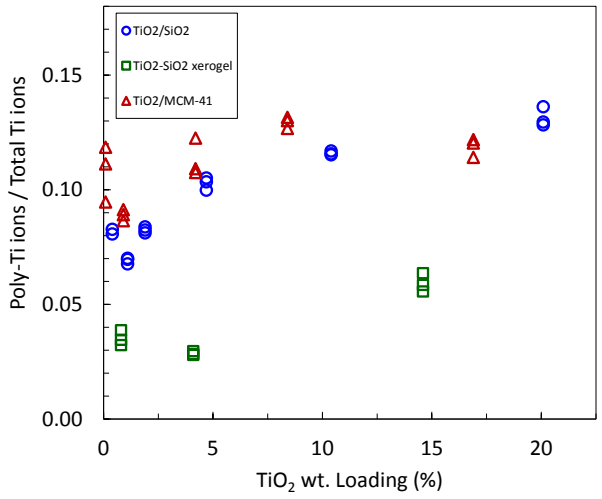

Figure 4. Relative proportion of "Poly Ti" ions ($Ti_2O_2^+$, $Ti_2O_3^+$, $Ti_2O_4H^+$, $Ti_3O_3^+$, $Ti_3O_4^+$, $Ti_3O_5^+$, $Ti_4O_6^+$, $Ti_4O_7^+$) detected at the surface of all catalysts by ToF-SIMS, as a function of the TiO_2 loading. Each catalysts has been analyzed on three spots. The counts for all "Poly Ti" ions are pooled together and normalized by the total count for all ions containing Ti to get a relative value of the signal for condensed Ti species.

$Ti_3O_3^+$, $Ti_3O_4^+$, $Ti_3O_5^+$, $Ti_4O_6^+$, $Ti_4O_7^+$) are detected in higher proportions, accounting for the occurrence of condensed (oligomeric or polymeric) surface species (Figure 4). This trend is visualized by comparing the signals of two representative ions (e.g. $Ti_2O_2^+$ and $TiSiO_2^+$) for different samples at similar TiO_2 loading: the dimeric titanate ion is not detected on the xerogel when it is detected on the impregnated catalysts (Fig. S7). Clearly, ToF-SIMS indicates that the dispersion of Ti is higher in the xerogels, but with a lower amount of Ti available at the surface. Also, both series of impregnated catalysts feature a similar degree of TiO_x condensation at the outermost surface, but with probably a higher proportion of TiO_2 incorporated into the pores of MCM-41 and not probed by this technique acting at the external surface of the particles.

DR UV-VIS spectroscopy is a useful tool to provide information on the coordination geometry of the Ti cations and ligand environment through the energy position of the ligand-to-metal charge transfers (O→M LMCT). For the dried TiO_2/SiO_2 catalysts (Figure 5A), an LMCT transition band was observed at ~43,800 cm^{-1} at the lowest TiO_2 loadings. LMCT transitions at 45,000-41,000 cm^{-1} have been commonly attributed to tetrahedral TiO_4 species in dehydrated TiO_2-SiO_2 mixed and TiO_2/SiO_2 supported oxides.[25,27,36,37] For increasing TiO_2 loadings, a red-shift of the LMCT transition is observed according to an increase in Ti-polymerization.[25,27,36] In order, three new signals are observed at ~37,500, ~36,300 and ~31,000 cm^{-1}, which have been attributed to dimeric or one-dimensional polymerized TiO_4 units, two-dimensional polymerized TiO_5 units

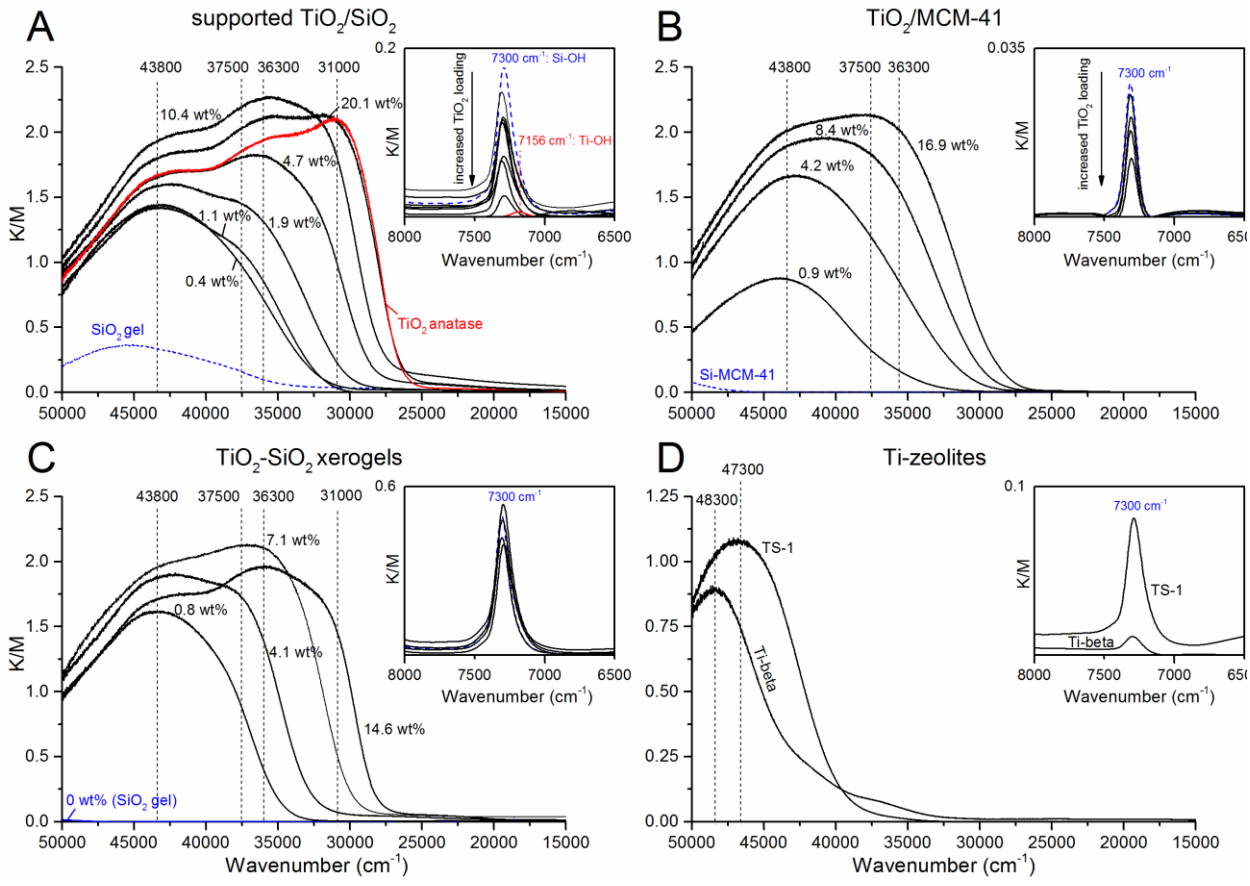

Figure 5. DR UV-VIS spectra of A) TiO_2/SiO_2, B) TiO_2/MCM-41, C) TiO_2-SiO_2 xerogels and D) Ti-zeolites. Insets show the silanol region of the same spectra.

and octahedral TiO_6 units (similar as in bulk TiO_2), respectively.[25,27] The observation of the presence of anatase at a 20.1 wt% TiO_2 loading is in agreement with the above-described Raman spectra. The decreasing absorption at 7300 cm^{-1} (inset of A) for increasing TiO_2 loadings suggests the gradual coverage of surface Si-OH groups by TiO_2. No absorption signals attributed to Ti-OH groups (located at 7156 cm^{-1}) was observed most likely due to their instability at temperatures higher than 180 °C.[38] Only for anatase, a weak Ti-OH signal was recognized. The absence of signals at 7140, 6881 and 5271 cm^{-1}, associated with physisorbed H_2O molecules (Figure S8), indicates that the samples were dry after pretreatment. A similar red-shift of LMCT transitions was noticed for TiO_2/MCM-41 (Figure 5B), albeit less extensive. The larger surface area of the Si-MCM-41 support compared to the SiO_2 gel allows a better dispersion of Ti species. Hence, no LMCT transition at ~31,000 cm^{-1} corresponding to TiO_6 units was observed, even at 17 wt% TiO_2 loadings. Compared to TiO_2/SiO_2, a slighter decrease in the amount of surface Si-OH groups was observed for increased TiO_2 loadings as shown by the decreasing 7300 cm $^{-1}$ band (inset of Figure 5B). In contrast, no significant decrease of the silanol signal at 7300 cm^{-1} was observed for TiO_2-SiO_2 gels, conform to the dispersion of Ti atoms in the bulk matrix instead of on the surface (inset Figure 5C). Similar to TiO_2/MCM-41, the red-shift of the LMCT transition occurs more slowly for increased TiO_2 loadings in the TiO_2–SiO_2 gel, when compared to TiO_2/SiO_2. The Ti-zeolites (Figure 5D) exhibited a narrow LMCT band centered around 48,300 and 47,300 cm^{-1} for Ti-beta and TS-1, respectively, which has been attributed to isolated tetrahedral framework TiO_4 units.[22,26,39] LMCT transitions assigned to tetrahedral TiO_4 species in Ti-zeolites are commonly observed at higher wavenumbers than in supported or mixed oxides.[25,36,40] It has been proposed that this difference is due to larger Ti-O-Si bond angles[41] or the presence of small fractions of octahedrally coordinated Ti species, even at very low Ti contents for supported or mixed oxides.[25,41,42]

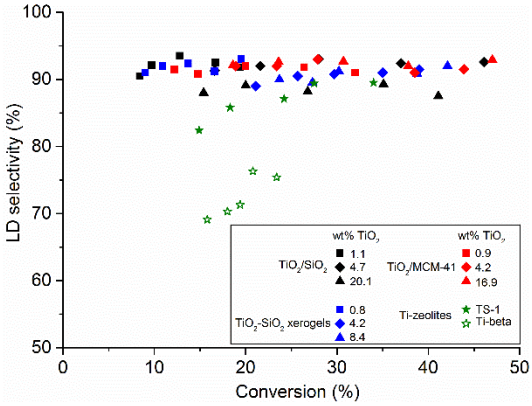

Figure 6. Conversion-selectivity plot for the gas-phase transesterification of L-MLA to LD by different Ti-Si catalysts. Reaction conditions: 5.7% L-MLA in N_2, 220-260 °C, WHSV = 15.53 h^{-1}.

The low intensity of the silanol band at 7300 cm^{-1} of Ti-beta accounts for the hydrophobic character of Ti-beta synthesized in fluoride media.[22,27].

Catalyst testing. The selectivity of the different catalyst types was compared for the gas-phase transesterification of L-MLA to LD at varying conversion. TiO_2 supported on MCM-41 and the mixed xerogels exhibit a high LD selectivity (86-92%), comparable to the TiO_2/SiO_2 reference catalyst, and irrespective of catalyst loading (Figure 6 and Table S1). LD selectivity was slightly lower for TS-1 at low conversion levels (< 20%) due to higher amounts of the linear dimer ester (ML_2A, Table S1, entry 4), but eventually also increased to ~88% at conversions above 20%. For Ti-beta however, LD selectivity was significantly lower due to a more pronounced etherification of MLA with MeOH to methyl-2-methoxy propionate (M_2MP, Table S1, entry 5). In agreement with our previous study[8], MLA conversion was thermodynamically limited around ~50%, due to the reaction reaching equilibrium (e.g., for TiO_2-SiO_2, Figure S9).

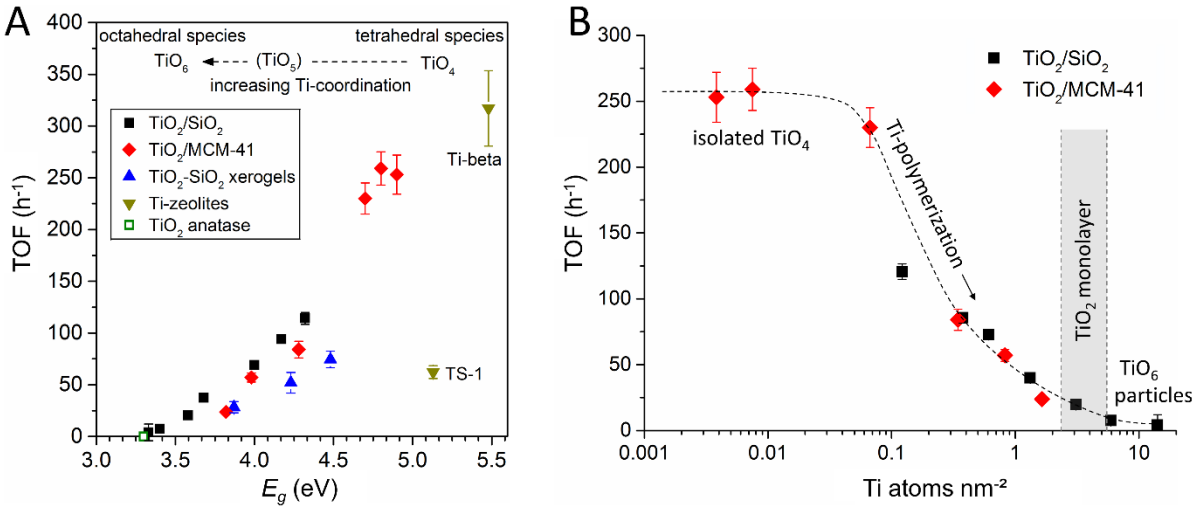

Figure 7. A) Influence of the catalyst's E_g on the corresponding TOF for different types of Ti-Si catalysts for the gas-phase transesterification of MLA to LD. Reaction conditions: 5.7% L-MLA in N2, 220 °C, WHSV = 15.5 h^{-1}. B) Catalyst's TOF as a function of the Ti dispersion on the catalyst surface. The dashed line is a guide to the eye. Reaction conditions: 5.7% L-MLA in N2, 220 °C, WHSV = 15.5 h^{-1}. TiO_2 monolayer region was designated based on literature values.[27,32,33] Plotted data points and side bars (not visible when they are thinner than the data point) are the average values and standard deviation of three identical runs, respectively.

Racemization was low, showing ≤ 6% meso-LD at conversions below 50% for all catalyst types (Figure S10). Ti-free analogues did not show any significant LD formation (Table S2).

Ti-coordination and catalytic activity. In continuation of our previous work[8], we investigated the specific catalytic activity of each catalyst type in relation to the corresponding band gap energy (E_g). The latter was calculated from the optical absorption edges in the DR UV-VIS spectra of Figure 5 (see Figure S11 for details about the method). The value of E_g is related to significant dimensional, structural and/or functional properties and is dependent on the number of nearest MO_x polyhedral neighbors and the number of bonds between each of those neighbors.[19] Thus, the evolution of the structure/coordination of supported Ti-cations as a function of loading can be traced by their corresponding E_g values. Generally, a monotonic increase in the TOF (mol MLA converted per mol Ti per hour) was observed for an increased E_g (and thus, a decrease in average Ti-coordination) for all catalyst types (Figure 7A). TiO_2 supported on SiO_2 or MCM-41 acted very similarly, with a continuous increase of the catalyst's TOF from 4 to 253 h^{-1} for an E_g of 3.33 to 4.9 eV, respectively. A similar increase was noted for TiO_2-SiO_2 gels. However, since this catalyst contains Ti-atoms within the bulk matrix of the gel unable to participate in the reaction, TOF values for the TiO_2-SiO_2 gels are underestimated. Unfortunately, a precise determination of accessible Ti-sites remains difficult. The highest TOF was observed for the Ti-beta zeolite: with ~5.5 eV E_g, a TOF of 317 h^{-1} was calculated. TS-1 on the other hand exhibited a TOF that was exceptionally lower than expected from its E_g, which might indicate diffusional limitations due to its small pore size. The relatively high apparent activation energy (*vide infra*) calculated for this catalyst on the other hand does not support this. Generally, tetrahedral TiO_4 sites are catalytically more active than their polymerized counterparts having a typically higher Ti-coordination. Indeed, a plot of TOF as a function of Ti dispersion for the supported catalysts further helps visualizing this trend (Figure 7B). In the sub-monolayer region (under 2.2 – 5.5 Ti atoms nm^{-2})[27,32,33], the TOF continuously increases until reaching a plateau around ~250 h^{-1} for very disperse, SiO_2-supported catalysts (0.05-0.1 wt% TiO_2), corresponding to the apparent, intrinsic catalytic activity of isolated tetrahedral TiO_4 sites. The high surface area of the MCM-41 support allows for a much larger Ti dispersion and hence, allows the catalyst to operate under TOFs that are approx. 2.5 times higher compared to TiO_2/SiO_2 with similar TiO_2 loadings (Figure 8). Accordingly, the space time yields (STY) of LD increased from 1.6 to 3.3 g_{LD} g_{cat} h^{-1} at 220 °C. At 260 °C, LD STY nearly reached 10 g_{LD} g_{cat}^{-1} h^{-1} using a TiO_2/MCM-41 catalyst, compared to ≤ 4 g_{LD} g_{cat} h^{-1} for TiO_2/SiO_2, TiO_2-SiO_2 xerogels or Ti-zeolites (Figure S12-13).

Kinetic analysis. As the specific catalytic activity was strongly correlated to TiO_2 loading, no significant changes in apparent activation energy (E_a) were observed from the corresponding Arrhenius plots for the supported catalysts (Figure 9 A-B). Irrespective of catalyst loading, E_a values

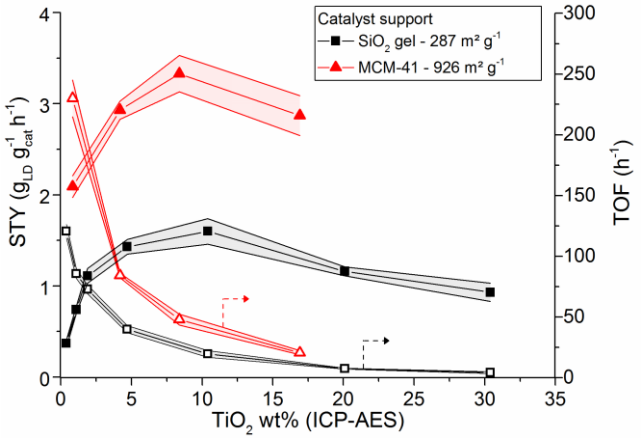

Figure 8. Comparison of STY and TOF for TiO_2/SiO_2 and TiO_2/MCM-41 with similar TiO_2 loadings. Dots and connected lines indicate the average and standard deviation of 3 identical measurements respectively. Full symbols: STY, open symbols: TOF. Reaction conditions: 5.7% L-MLA in N_2, 220 °C, WHSV = 15.5 h^{-1}.

around 49-56 kJ mol^{-1} were calculated for TiO_2/SiO_2 and TiO_2/MCM-41. A slightly lower E_a of ~35 kJ mol^{-1} was determined for the TiO_2-SiO_2 xerogels, irrespective of the TiO_2 loading (Figure 9C). The TS-1 zeolite exhibited an E_a of 49.5 kJ mol^{-1}, a value similar to the supported oxides (Figure

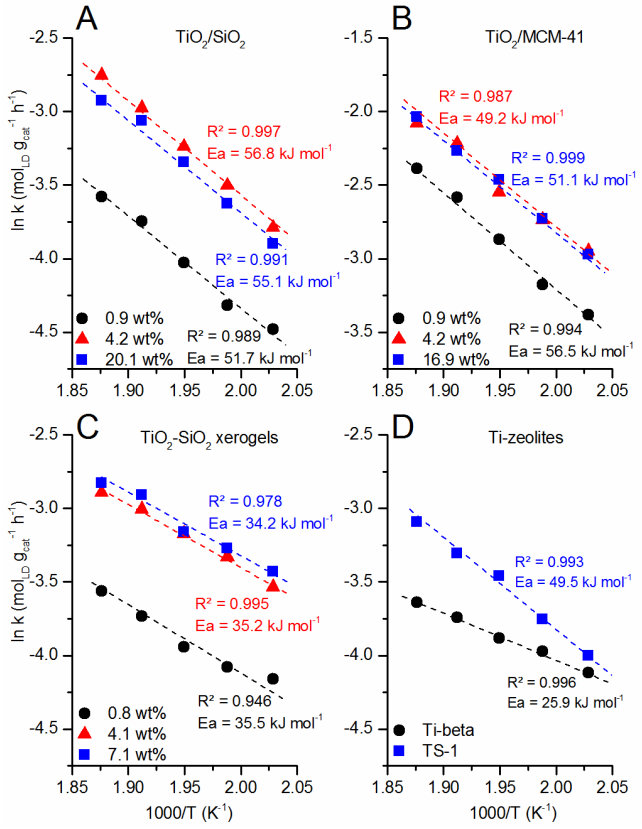

Figure 9. Arrhenius plots for the conversion of L-MLA to LD by A) TiO_2/SiO_2, B) TiO_2/MCM-41, C) TiO_2-SiO_2 xerogels and D) Ti-zeolites. Reaction conditions: 5.7% L-MLA in N_2, 220-260 °C, WHSV = 15.5 h^{-1}.

9D). The E_a of Ti-beta was, on the other hand, significantly lower, *viz.* 25.9 kJ mol^{-1}. It is unclear whether this low E_a is due to Ti-beta truly decreasing the energy barrier of MLA conversion, or due to the presence of diffusional limitations (suggested by the $E_a/2$ rule). Zeolite crystals synthesized in fluoride-containing media typically reach side length of > 6 μm in size, much larger than the TS-1 particles synthesized in basic, OH^--rich media (< 1 μm).[21] Thus, intraparticle diffusion limitations could be induced, even though the pore size of the BEA zeolites is larger than those of the MFI topology. No interparticle or film diffusional limitations were experimentally observed (Table S3), but intrazeolitic diffusional limitations could not be excluded with this test. However, since Ti-beta was less selective to LD compared to the other catalysts, we did not further investigate this matter. E_a is found to be invariable with TiO_2 loading for supported and gel catalysts. The difference in kinetics thus originates from the pre-exponential factor *k*, derived from the intercept of the Arrhenius plot with the y-axis. Among other factors, the pre-exponential factor is dependent on the number of and on the collision frequency of reagents with active sites. Therefore, we propose that the catalytic activity of TiO_2-based catalysts for the transesterification of MLA to LD is proportional with the number (accessibility) of vacant sites on the TiO_2 surface. Tetrahedral TiO_4 units offer 2 vacant sites, whereas octahedral TiO_6 units have none. An increased TiO_2 dispersion decreases the average coordination of Ti and, thus, increases the number of vacant sites. The increased activity of tetrahedral Ti-sites compared to octahedral sites does not seem to be due to any mechanistic changes of the reaction or the active site itself, as differences in E_a would then be expected. LD productivities may therefore be significantly increased by the use of SiO_2 supports having high surface areas, for example ordered mesoporous materials such as MCM-41.

CONCLUSION

Different Ti-Si catalysts, *viz.* TiO_2 supported on amorphous SiO_2 or Si-MCM-41; TiO_2-SiO_2 xerogels and Ti-zeolites (TS-1 and Ti-beta) were tested for the gas-phase transesterification of MLA to LD. In all catalysts, covalent Ti-O-Si bonds between the Ti active sites and the SiO_2 support structure were present. With the exception of Ti-beta, all catalyst types exhibit a high LD selectivity of 85-92 % at conversions below 50%. Irrespective of the catalyst structure, an increased band gap energy, as derived from the optical absorption edge from DR UV-VIS spectra, correlated with a higher turnover frequency of the Ti-sites. Tetrahedral TiO_4 sites are more active for MLA transesterification than polymerized TiO_5 or TiO_6 counterparts (ToF-SIMS measurements confirmed this degree of Ti-polymerization on the surface). This behavior explains the sigmoidal correlation between Ti surface density and the TOF (Fig. 7B) for supported Ti catalysts, spanning from amorphous to MCM-41 siliceous supports. No changes in apparent activation energy were observed upon increasing TiO_2 loadings, suggesting that the catalytic activity is proportional to the number of vacant reactive sites on the TiO_2 surface and is not due to any mechanistic changes of the reaction/active site itself. Therefore, the preferred catalyst for LD production from MLA is featured by a high dispersion of the TiO_2 phase on the SiO_2 surface. Using these guidelines, by supporting TiO_2 on an MCM-41 support, having a higher specific surface area than amorphous SiO_2 gel, turnover numbers and consequently, LD productivity, is increased up to 2.5 times for similar TiO_2 loadings, compared to an amorphous SiO_2 gel with a smaller surface area and thus lower dispersion of the catalytically active TiO_2 phase.

ASSOCIATED CONTENT

Supporting Information. Powder XRD patterns, Raman spectra and other additional characterization results (XPS, DR UV-VIS) and additional catalytic data are given in the supporting information. This material is available free of charge via the Internet at http://pubs.acs.org.

AUTHOR INFORMATION

Corresponding Author

* E-mail: michiel.dusselier@kuleuven.be
bert.sels@kuleuven.be

Notes

The authors declare no competing financial interest.

ACKNOWLEDGMENT

R.D.C. acknowledges IWT (Agency for Innovation by Science and Technology, project number 131404) for financial support. M.D. thanks Research Foundation - Flanders (FWO, 12E8617N) for funding and KU Leuven BOF for his appointment to Research Professor. M.D., E.M. and B.F.S. thank the Industrial Research Fund (IOF, grant ZKC8139).

REFERENCES

(1) Law, K. L.; Thompson, R. C. *Science* **2014**, *345*, 144–145.
(2) Cózar, A.; Echevarría, F.; González-Gordillo, J. I.; Irigoien, X.; Úbeda, B.; Hernández-León, S.; Palma, Á. T.; Navarro, S.; García-de-Lomas, J.; Ruiz, A., Fernández-de-Puelles, M., Duarte, C. M. *Proc. Natl. Acad. Sci.* **2014**, *111*, 10239-10244.
(3) Zhu, Y.; Romain, C.; Williams, C. K. *Nature* **2016**, *540*, 354-362.
(4) De Clercq, R.; Dusselier, M.; Sels, B. F. *Green Chem.* **2017**, *19*, 5012–5040.
(5) Auras, R., Lim, L.-T., Selke, S. E. M., Tsuji, H., Eds.; Poly(Lactic Acid): Synthesis, Structures, Properties, Processing, and Applications; John Wiley & Sons Inc.: New York, 2010.
(6) Van Wouwe, P.; Dusselier, M.; Vanleeuw, E.; Sels, B. *ChemSusChem* **2016**, *9*, 907-921.
(7) Dusselier, M.; Van Wouwe, P.; Dewaele, A.; Jacobs, P. A.; Sels, B. F. *Science* **2015**, *349*, 78-80.
(8) De Clercq, R.; Dusselier, M.; Makshina, E.; Sels, B. F. *Angew. Chem. Int. Ed.* **2018**, *57*, 3074-3078.
(9) Bellis, H. E.; Bhatia, K. K. Continuous catalyzed vapor phase dimeric cyclic ester process. WO 92/00292, 1992.
(10) Benecke, H. P.; Markle, R. A.; Sinclair, R. G., EP 0 549 698 B1, 1994.
(11) Hölderlich, W.; Venschott, M. WO 2013/160485 A1, 2013.
(12) Upare, P. P.; Yoon, J. W.; Hwang, D. W.; Lee, U.-H.; Hwang, Y. K.; Hong, D.-Y.; Kim, J. C.; Lee, J. H.; Kwak, S. K.; Shin, H.; Kim, H.; Chang, J.-S. *Green Chem.* **2016**, *18*, 5978–5983.

(13) Feng, L.; Chen, X.; Sun, B.; Bian, X.; Chen, Z. *Polym. Degrad. Stab.* **2011**, *96*, 1745–1750.
(14) Kamble, S. P.; Barve, P. P.; Joshi, J. B.; Rahman, I.; Kulkarni, B. D. *Ind. Eng. Chem. Res.* **2012**, *51*, 1506.
(15) Holm, M. S.; Saravanamurugan, S.; Taarning, E. *Science* **2010**, *328*, 602-605.
(16) Murphy, B. M.; Letterio, M. P.; Xu, B. *J. Catal.* **2016**, *339*, 21–30.
(17) Murphy, B. M.; Letterio, M. P.; Xu, B. *ACS Catal.* **2016**, *6*, 5117–5131.
(18) Murphy, B. M.; Letterio, M. P.; Xu, B. *ACS Catal.* **2017**, *7*, 1912–1930.
(19) Martra, G.; Gianotti, E.; Coluccia, S. In *Metal Oxide Catalysis*; (Eds: Jackson, D. S., Hargreaves, J. S. J.); Wiley-VCH, Weinheim, 2009; pp 51–94.
(20) Aguado, J.; Vangrieken, R.; Lopezmunoz, M.; Marugan, J. *Appl. Catal. A Gen.* **2006**, *312*, 202–212.
(21) Carati, A.; Berti, F. D.; Millini, R.; Stocchi, B.; Perego, C. In *Porous Materials in Environmentally Friendly Processes*; (Eds: Kiricsi, I., Pál-Borbély, G., Nagy, J. B., Karge, H. G.), Elsevier Science B.V., 1999; Vol. 125, pp 45–52.
(22) Blasco, T.; Camblor, M. A.; Corma, A.; Esteve, P.; Martinez, A.; Prietob, C.; Valencia, S. *Chem. Commun.* **1996**, *3*, 2367–2368.
(23) Caillot, M.; Chaumonnot, A.; Digne, M.; Poleunis, C.; Debecker, D. P.; van Bokhoven, J. A. *Microp. Mesop. Mater.* **2014**, *185*, 179–189.
(24) International Zeolite Association: Structure commission. *Database of Zeolite Structures,* Http://Www.Iza-Structure.Org/Databases/.
(25) Gao, X.; Wachs, I. E. *Catal. Today* **1999**, *51*, 233–254.
(26) Boccuti, M. R.; Rao, K. M.; Zecchina, A.; Leofanti, G.; Petrini, G. In *Structure and Reactivity of Surfaces* (Eds: Morterra C., Zecchina A., Costa, G.); Elsevier: Amsterdam, 1989, pp 133–144.
(27) Gao, X.; Bare, S. R.; Fierro, J. L. G.; Bañares, M. A.; Wachs, I. E. *J. Phys. Chem. B* **1998**, *102*, 5653–5666.
(28) Dutoit, D. C. M.; Schneider, M.; Baiker, A. *J. Catal.* **1995**, *1*, 165–176.
(29) Chmel, A.; Eranosyan, G. M.; Kharshak, A. A. *J. Non-cryst. Solids* **1992**, *146*, 213–217.
(30) Salvado, M. I. M.; Navarro, F. J. M. *J. Non-cryst. Solids* **1992**, *147-148*, 256–261.
(31) Castillo, R.; Koch, B.; Ruiz, P.; Delmon, B. *J. Catal.* **1996**, *161*, 524–529.
(32) Cozzolino, M.; Di Serio, M.; Tesser, R.; Santacesaria, E. *Appl. Catal. A Gen.* **2007**, *325*, 256–262.
(33) Muñoz-Paez, A.; Munuera, G. In *Studies in Surface Science and Catalysis Vol. 63*; (Eds: Poncelet, G., Jacobs, P. A., Delmon, B.); Elsevier: Amstersdam, 1991, pp 627–363.
(34) Weng, L. *Appl. Catal. A Gen.* **2014**, *474*, 203–210.
(35) Bouchmella, K.; Mutin, P. H.; Stoyanova, M.; Poleunis, C.; Eloy, P.; Rodemerck, U.; Gaigneaux, E. M.; Debecker, D. P. *J. Catal.* **2013**, *301*, 233–241.
(36) Klein, S.; Weckhuysen, B.; Martens, J. *J. Catal.* **1996**, *491*, 489–491.
(37) Lu, J.; Kosuda, K. M.; Van Duyne, R. P.; Stair, P. C. *J. Phys. Chem. C* **2009**, *113*, 12412–12418.
(38) Haukka, S.; Lakomaa, E.-L.; Root, A. *J. Phys. Chem.* **1993**, *97*, 5085–5094.
(39) Camblor, M. A.; Costantini, M.; Corma, A.; Gilbert, L.; Esteve, P.; Martinez, A.; Valencia, S. *Chem. Commun.* **1996**, 1339–1340.
(40) Liu, Z.; Crumbaugh, G. M.; Davis, R. J. *J. Catal.* **1996**, *159*, 83–89.
(41) Greegor, R. B.; Lytle, F. W. *J. Non-cryst. Solids* **1983**, *55*, 27–43.
(42) Liu, Z.; Tabora, J.; Davis, R. J. *J. Catal.* **1994**, *149*, 117–126.
(43) Van Wouwe, P.; Dusselier, M.; Basiç, A.; Sels, B. F. *Green Chem.* **2013**, *15*, 2817-2824.

Table of contents artwork: